Development of a Small-Scale Test Facility for Effectiveness Evaluation of Fixed-Bed Regenerators

Easwaran N Krishnan[1*], Hadi Ramin[1], Mohsen Shakouri[2], Lee D Wilson[3] and Carey J Simonson[1]
[1]Department of Mechanical Engineering, University of Saskatchewan, 57 Campus Drive, Saskatoon, SK S7N 5A9, Canada
[2]Canadian Light Source Inc., 44 Innovation Boulevard, Saskatoon, SK S7N 2V3, Canada
[3]Department of Chemistry, University of Saskatchewan, 110 Science Place, Saskatoon, SK S7N 5C9, Canada
[*]**Corresponding author Email:**enk133@mail.usask.ca

Abstract

Fixed-bed regenerators (FBR) transfer heat (and moisture) between supply and exhaust air streams in heating, ventilating and air conditioning (HVAC) systems to reduce building energy consumption. This paper presents a new small-scale testing facility to evaluate the performance (i.e. sensible effectiveness) of FBRs for HVAC applications. The major contributions of this paper are: development of a new small-scale experimental facility and methodology for testing FBRs, quantification of uncertainties, and verification of small-scale test data over a large range of FBR design conditions. A numerical model and two well-known design correlations are used to verify the results and testing methodology. The advantages of small-scale testing are that it requires low volume of conditioned airflow, has low uncertainty, requires less exchanger material and has a low cost per test. Moreover, the small-scale testing methodology of FBR would benefit heat exchanger manufacturers to perform detailed sensitivity studies and optimize the exchanger performance over a wide range of design and operating parameters prior to the fabrication of full-scale exchangers.

Keywords: Fixed-bed regenerators; Performance testing; Sensible effectiveness; Heat recovery; HVAC.

Nomenclature

FBR	fixed-bed regenerator	T	instantaneous temperature (°C)
A	total heat transfer area of the exchanger (m^2)	$\overline{T}$	average temperature (°C)
C	heat capacity rate (J/s K)	U	total uncertainty

C_p	specific heat capacity (J/K)	$x_{h,FD}$	hydrodynamic entry length (m)
Cr*	heat capacity rate ratio	$x_{th,FD}$	thermal entry length (m)
Ex	exchanger	**Greek symbols**	
h	convective heat transfer coefficient ($W/m^2 K$)	ε	sensible effectiveness (%)
k	thermal conductivity (W/m K)	ρ	density (kg/m^3)
L	exchanger length (m)	λ	longitudinal heat conduction factor
LAU	linear actuator unit	**Subscript**	
NTU_o	number of transfer units	ch	channels
P	period (s)	FD	fully developed
Pe	Peclet number	g	bulk air
Re	Reynolds number	i	exchanger inlet
RH	relative humidity (%)	m	matrix
t_s	student t-factor	o	exchanger outlet

1. Introduction

Global energy consumption is continuously increasing because of population growth and developments in infrastructure. In developed countries, approximately 40% of total energy is consumed in buildings while more than half of this energy is used in HVAC systems [1]. Moreover, HVAC systems and refrigerants have some adverse effects such as air pollution and greenhouse gas emissions [2]. On the other hand, many studies have already shown that thermal comfort and indoor air quality have a significant impact on health and productivity [3]. Therefore, HVAC system designers and researchers have a great interest in developing energy-efficient and environmental-friendly technologies without compromising thermal comfort and indoor air quality in buildings. Current HVAC systems often include air-to-air energy exchanger to improve the system efficiency by utilizing the energy of building exhaust to condition the supply air [4–6]. Air-to-air energy exchangers reduce the load on the HVAC unit thus lowering the size of the unit as

well as the energy consumption. The selection of a suitable energy exchanger is based on climate data, application, indoor and outdoor conditions and maintenance cost [7,8].

Fixed-bed regenerators (FBR) are air-to-air energy exchangers that have been used in various industries since 1960 [9,10]. The schematic of an FBR with two exchangers (EX), two fans, and a damper assembly is shown in Fig. 1. One complete operation of an FBR can be divided into two periods. During the first half of the operation (period 1), the dampers are positioned vertically as shown in Fig.1(a). For the case of winter operation (cold outdoor air), exchanger 1 (EX 1) will heat the supply air stream. Simultaneously, exchanger 2 (EX 2) will store heat from the return air stream. At the end of period 1, the dampers rotate 90^{o} to the position as

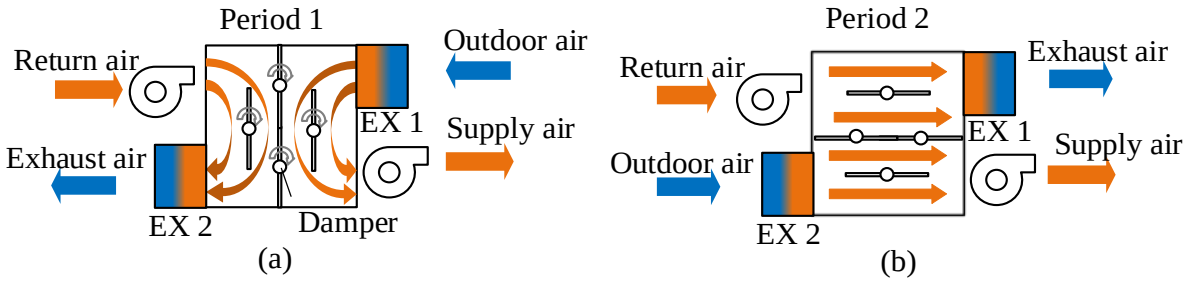

Fig. 1. Schematic showing the operation of an FBR with two stationary energy exchangers.

shown in Fig.1(b). During the second period, EX 2 will release the energy stored during the first period to heat the cold outdoor airstream. The duration of each period is generally about 60 seconds [11] and the two periods repeat alternatively to deliver conditioned outdoor air continuously to the building. Rotary and flat plate exchangers are widely implemented in commercial HVAC systems [12]. Compared to rotary and flat plate exchangers, FBRs have low maintenance, high heat transfer effectiveness [13] and they are less susceptible to frost formation during the winter operation since the air flow reverses after every period.

Several numerical and analytical studies assessing the performance of FBRs for high-temperature applications such as power-plants [14], glass manufacturing [15] and process industries [16] have been reported in the literature. However, there are only limited literature have addressed the performance of FBRs experimentally in HVAC applications. Chang et al. [17] used an experimental approach to evaluate the performance of an FBR unit consisting of two desiccant-coated stationary wheels. They determined the optimum duration of heating and cooling periods required to obtain maximum total effectiveness using different desiccant composites [18]. Aristov et al. [19] developed an FBR with a single exchanger consisting of heat and moisture storage materials. Their device achieved sensible and latent effectiveness of 85 % and 60 %, respectively,

during winter tests in Russia [6]. The possibility of using FBRs for room ventilation was evaluated numerically by Nizotsev et al. [20]. Their results were validated experimentally in a single-exchanger FBR test setup using a reversible fan. However, all the studies mentioned above require extensive test facilities and full-scale/practical FBR units.

The performance of FBRs in HVAC applications can be determined experimentally following the guidelines provided by the CSA 439-18 [21] standard with an acceptable range of uncertainties. Standard methods to evaluate the performance of full-scale FBRs are challenging since they require large laboratory spaces, high volume of airflow rates and extensive testing facilities. Because of these limitations of standard testing methodology of energy exchangers, researchers have been seeking alternative methods for performance evaluation and product development [22,23]

Recent studies show that the performance of energy exchangers can be predicted by testing either a portion of the exchanger or a small-scale prototype [24]. Abe et al. [25] and Wang et al. [26] have studied the transient temperature and humidity response of an energy wheel subjected to temperature and humidity step changes. These tests were performed using only a portion of the wheel to predict the sensible and latent effectiveness of full-size energy wheels from the transient temperature and humidity responses, respectively. Recently, Fatheih et al. [27,28] predicted the performance of rotary heat wheels by measuring the transient response of a small-scale heat exchanger subjected to step changes in the inlet stream condition. Later, Shakouri et al. [29,30] showed that the latent effectiveness of an energy wheel could be determined accurately from small-scale tests. Similar to rotary regenerators, the performance of liquid to air membrane energy exchangers (LAMEE) has also been determined through testing a small-scale LAMEE exchanger [31]. Through LAMEE performance evaluation, Moghaddam et al. [32] developed a testing methodology for energy exchangers using nondimensional performance parameters such as the overall number of transfer units (NTU_o) and heat capacity rate ratio (Cr^*).

The main objectives of this paper are: (i) to introduce and commission a new test facility to determine the sensible effectiveness of FBRs at different operating conditions, (ii) to test the small-scale facility, verify the testing methodology and quantify the uncertainty in sensible effectiveness at different operating conditions. The significance of temperature measurements, effects of operating conditions such as the duration of heating/cooling period and face velocity of the inlet airstreams on sensible effectiveness are also studied. Finally, the results are presented

using nondimensional performance parameters and compared with a numerical model and design correlations from the literature.

2. Experimental Facility

The principle of operation of the test facility, where the small-scale parallel-plate exchanger and the experimental procedures will be presented in the following subsections.

2.1. Small-scale FBR test facility

The small-scale test facility is designed to simulate the cyclical operation of an FBR in practice by moving a small-scale exchanger between two air streams having different temperatures as shown in Fig. 2. The properties of air streams at the inlet and outlet of the exchanger are measured to determine the performance of the small-scale exchangers.

The test facility comprises a supply air system and a test section. The function of supply air system is to provide conditioned air to the test section, where the small-scale exchanger is located. The test facility is capable of testing FBRs with different geometrical configurations.

2.1.1 Supply air system

Two centrifugal blowers are used to supply air to the test section. The air supply lines are made of circular PVC pipes with 50.8 mm (2 in.) inner diameter. The required flow rate is maintained by adjusting the rotational speed of blowers using variable voltage transformers. The airflow is measured by measuring the pressure drop across an orifice plate located in each supply line. The overall uncertainty in the airflow rate measurement is ± 1.4 % mainly due to the ±12 Pa uncertainty in the pressure transducers. Honeycomb flow straighteners are installed at the blower outlets to enable accurate airflow rate measurements. The orifice plates and flow straighteners are designed in accordance with the ISO standard 5167-1 [33,34]. A tubular electric heater is placed at one of the air supply lines to heat the incoming air stream. The heater is controlled with a PID controller to maintain a constant temperature at the test section inlet with a maximum deviation of ±0.3°C. The supply air system can provide an airflow rate of 5.8-15 L/s in the range of -25 to 60°C. For a small-scale heat exchanger with a face area of 56 cm^2, the airflow rate corresponds to an exchanger face velocity of 0.8 to 2.5 m/s (157.5 to 492 fpm).

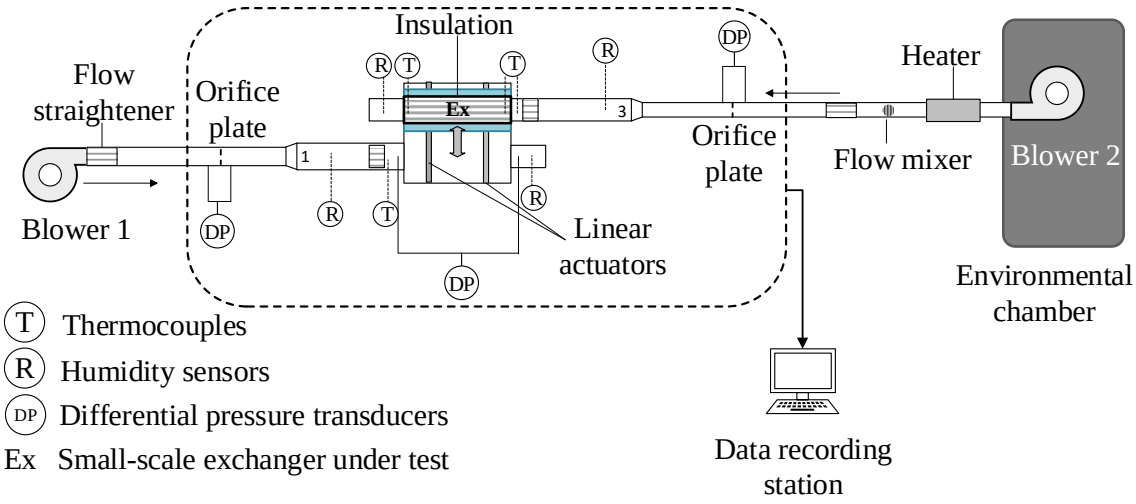

Fig. 2. Schematic of the small-scale FBR testing facility.

The air supply lines are connected to rectangular plexiglass ducts with a length of 700 mm shown as duct 1 and duct 3 in Fig. 2. These ducts are 80 mm × 70 mm inner cross section to match the size and geometry of test section to maintain uniform flow as the flow enters the test section. The two inlet ducts are insulated with 25.4 mm thick (1 in.) extruded polystyrene to reduce heat losses/gains to/from the surrounding environment. A flow mixer and flow straightener are placed inside each supply line (duct 1 and duct 3) to obtain a uniform flow velocity and uniform temperature at the test section inlet. The flow straighteners are composed of hundreds of 2 mm × 3 mm rectangular channels with a length of 100 mm.

2.1.2 Test Section

The function of the test section is to hold the small-scale exchanger and simulate the full-scale FBR operation by cycling the exchanger between the hot and cold airstreams. The test section includes an insulated PVC box, where the exchanger is located, and a linear actuator unit (LAU) as shown in Fig. 3. The LAU is an integral part of the test section that consists of two linear actuators, an air-filter pressure regulator and a solenoid valve controlled by a programmable phidget. It enables the exchanger to slide between the air streams, and consequently, subjects the exchanger to continuous hot and cold periods. The rails and the cartridges of LAU are attached to the base of the test facility and the exterior of the exchanger frame box, respectively. LAU takes about 0.3 s to slide from one section to the other, and the sliding speed can be adjusted by controlling the air pressure to the actuators. The top face of the test section can be opened to add

or remove the small-scale exchanger and can accommodate exchangers having a length of up to 1 m.

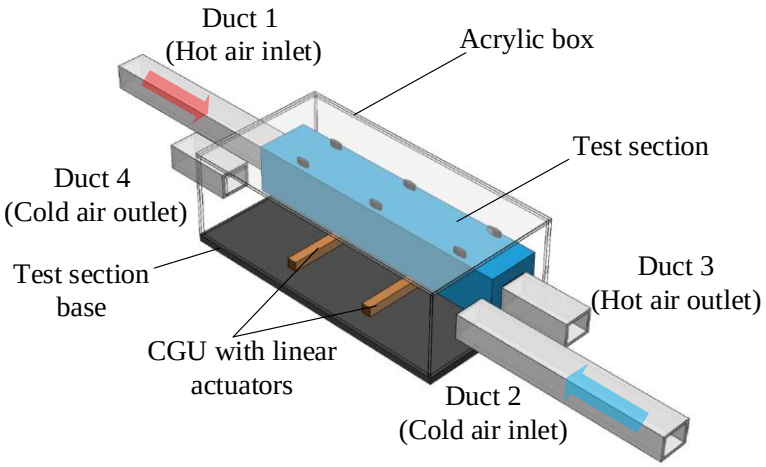

Fig. 3. Schematic of the test section of small-scale FBR facility.

The chances of air leakages at the exchanger inlets and outlets are critical since the test section slides between hot and cold airstreams alternatively. The leakage tests were performed at the beginning of experiments by injecting smoke through the blower suction side using a fog machine (Intertek, 1000W) and visually observing the presence of smoke outside the test section. The leakages through the test section inlets and outlets were successfully eliminated by providing adequate rubber sealing at the test section outlets.

2.2. Small-scale exchanger

A small-scale exchanger (or FBR) made of parallel aluminum plates is used in this study. The exchanger consists of 26 equally spaced aluminum plates, as shown in Fig. 4. Each plate is 0.69 mm thick, 80 mm long, and 200 mm wide. A 3D printed ABS frame is used to hold the plates in an equally spaced (2.1 mm) parallel arrangement. Thus the 26 parallel plates assemble an FBR having 25 flow channels with a hydraulic diameter of 4.08 mm and a Reynolds number between 262 and 850. The geometrical and physical properties of the exchanger are given in Table 1.

During a test, the exchanger is located inside the test section and is periodically exposed to conditioned (hot and cold) airstreams with the help of LAU. When the test section is in-line with the hot air stream, the exchanger stores heat from the hot air (hot period) and releases this stored heat when it is exposed to the cold air stream (cold period), simulating the operation of an FBR in

practice. The exchanger is insulated using a 50 mm (2 in.) thick polystyrene insulation, which substantially reduces any heat transfer between the exchanger and its surroundings.

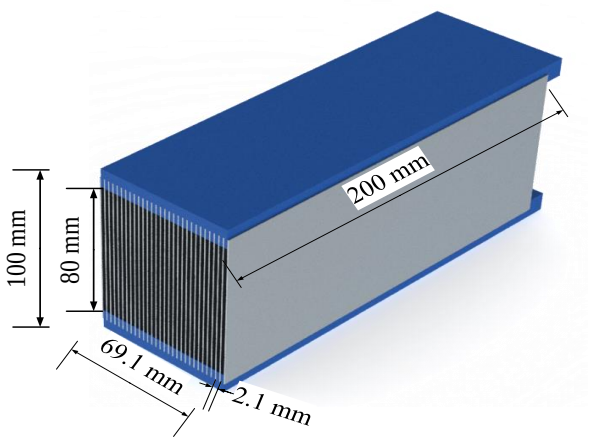

Fig. 4. The small-scale parallel-plate exchanger geometry with supporting frames (the uncertainty of length measurements is 0.05 mm for all the reported values).

Table 1. Geometrical details and thermophysical properties of the exchanger

Channel				Plates			
Length (mm)	Height (mm)	Width (mm)	Hydraulic diameter (mm)	Thickness (mm)	Thermal conductivity (W/m·K)	Density (kg/m^3)	Specific heat (J/kg·K)
200	80	2.1	4.08	0.69	162	2730	903

2.3. Measurements and data acquisition

2.3.1. Instrumentation and uncertainty analysis

The uncertainties in sensible effectiveness are calculated from the uncertainties in temperature and flow rate measurements. The uncertainties in measurements are obtained by calibrating the thermocouples, humidity sensors and pressure transducers using a dry-well temperature calibrator [35] (± 0.1ºC), Thunder scientific humidity generator [36] (±0.5% RH) and a precision portable pressure calibrator DPI 605 [37] (±1 Pa), respectively. During the calibrations, a sampling rate of 10 seconds is used to determine transients in temperature and humidity measurements. The uncertainties of measured variables are presented in Table 2.

Table 2. Instruments specifications and calibration details

Sl. No.	Instrument	Manufacturer/ type	Parameter	Capacity/ Calibration range	Total uncertinaty
1	Thermocouples	T-type/ (0.08mm wire dia.)	Temperature	20-60ºC	±0.2ºC
2	Pressure transducers	Validyne DP17	Differential pressure	0-860 Pa	12 Pa
3	Tubular heater	Omega (electric resistance)	-	0-600 W	-
4	Humidity sensors	Honeywell (capacitive type)	Relative humidity	15-85% at 25ºC and 35ºC	±1.5 %

The total uncertainty (U) in a measurement is determined from systematic (B_x) and random (P_x) uncertainties for 95% confidence intervals according to the ASME PTC standard 19.1 [38]:

$$U = \sqrt{P_x^{\,2} + B_x^{\,2}} \tag{1}$$

The random uncertainties (P_x) associated with all measured parameters are determined using Eqn. (2)

$$P_x = \frac{t_s \cdot SD}{N} \tag{2}$$

where t_s is the student t- factor at a 95% confidence interval for a degree of freedom of (N-1), and SD is the standard deviation of the measurements. Calibration and data reduction errors are included in the systematic uncertainty. The overall uncertainty in sensible effectiveness is determined using the method of uncertainty propagation rules as follows [39].

$$U_R = \left[\sum_{i=1}^{j}\left(\frac{\partial R}{\partial p_i} U_{p_i}\right)^2\right]^{0.5} \tag{3}$$

where U_R, U_{p_i}, and $\partial R/\partial p_i$ are the overall uncertainty, uncertainty associated with measurement property P_i and the sensitivity coefficient of measurement property P_i, respectively.

2.3.2 Temperature measurements and thermocouples arrangement

Since the exchanger periodically moves between two air streams, the outlet temperature continuously varies. Therefore, the sensors must respond quickly to obtain accurate measurements.

Calibrated T-type thermocouples are arranged in two different locations at the exchanger inlet and outlet for precise temperature measurements. The locations and configuration of thermocouples in the test facility are shown in Fig. 5. Four thermocouples which are 5 mm away from the exchanger

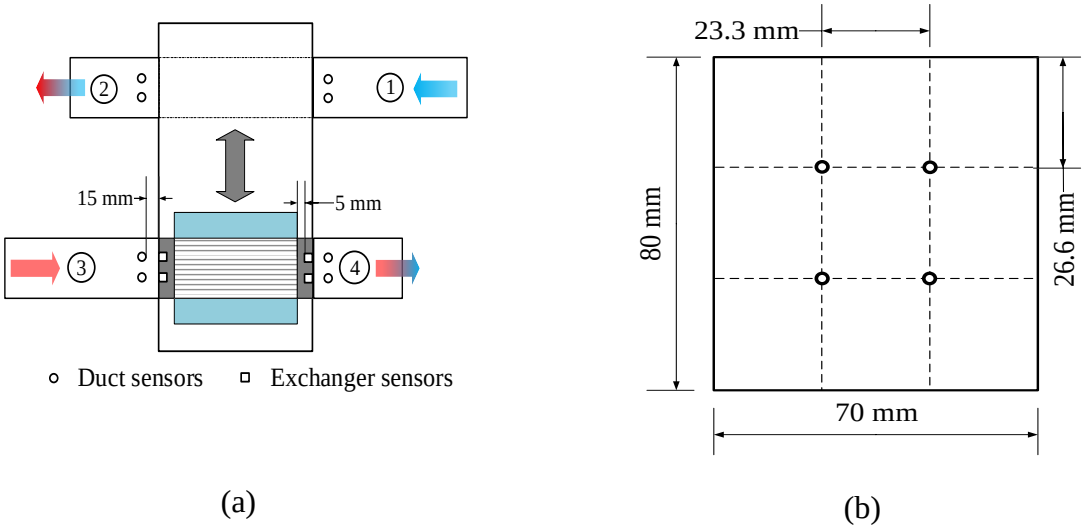

(a) (b)

Fig. 5. Schematic of the test facility showing thermocouples locations (a) and their spatial arrangements (b) at the exchanger inlet and outlet.

placed in the test section so that the sensors can move with the exchanger and hence named as exchanger sensors. Therefore the exchanger sensors measuring the temperature of the air at the exchanger inlets during one period measure the exchanger outlet air temperature in the adjacent period.

Additionally, four thermocouples are placed in each inlet and outlet duct, named duct sensors, which are stationary and exposed to the same kind of air stream always. For example, the sensors located in duct ④ will measure the exchanger outlet temperature during the hot period and measure the hot air inlet temperature during the cold period. The measured temperatures are recorded using a computer-controlled National Instruments data acquisition system (Chassis: NI SCXI-1000, modules: NI SCXI 1102, terminal blocks: NI SCXI-1303).

2.4. Experimental procedures

As described above, the supply air system provides the required airflow through the test section. One of the air streams is heated to 39 ±0.2°C (hot air stream) and other stream is kept at room temperature (cold air stream). Before every experiment, the conditioned air passes through the test section for at least one hour. When the variations in temperatures and flow rate

measurements become less than their measurement uncertainties for a period of 30 mins, it is assumed that the ducts and test section reach the steady-state condition. Then, the exchanger movement facilitates using LAU. The LAU slides the exchanger from one air stream to another in a very short time (approximately 0.3 seconds). After a series of cyclic exposures to hot and cold airstreams, the exchanger attains a quasi-steady state where the outlet temperature profile remains unchanged within the uncertainty of the measurements, for every period. The performance of FBR is then evaluated from quasi-steady-state outlet temperature profiles.

3. Numerical Model

In this study, a 1-D numerical model is used to verify the measured data from the small-scale FBR. The model considers laminar and incompressible flow through a representative parallel plate channel of the FBR (as shown in Fig. 6). The air and matrix material properties, and the mean air velocity are assumed to be constant and the model solves for bulk mean temperature of the air and the matrix (aluminum plate). The energy equations governing the heat transfer in one channel are [13]:

$$\rho_g C_{P_g} A_g \frac{\partial T_g}{\partial t} + U \rho_g C_{P_g} A_g \frac{\partial T_g}{\partial x} + h \frac{A_s}{L_{ch}} (T_g - T_m) = 0 \quad (4)$$

$$\rho_m C_{P_m} A_m \frac{\partial T_m}{\partial t} - h \frac{A_s}{L_{ch}} (T_g - T_m) = \frac{\partial}{\partial x} \left(k_m A_m \frac{\partial T_m}{\partial x} \right) \quad (5)$$

where: T, x, ρ, C_p, k, U, h, L and t are temperature, axial coordinate, density, specific heat capacity, thermal conductivity, mean airflow velocity, convective heat transfer coefficient, length of channel and time, respectively. The cross-sectional area of the air channel, heat transfer surface area and cross-sectional area of the matrix sheet are denoted as A_g, A_s and A_m, respectively. The subscripts 'g' and 'm' are used to refer to the bulk air and matrix properties, respectively. The energy equation for the airflow includes the storage, advection and convection, while the axial heat conduction is neglected because Pe>50. The energy equation for the matrix includes storage, convection, and axial conduction. The axial conduction term is particularly important for FBRs because they have thick matrix plates when compared to energy wheels. The assumptions used in the numerical model were reported and discussed in [40].

The boundary conditions are presented in Eqns. (6) and (7) must be satisfied for the supply and exhaust temperature [41].

$$T_g(0) = T_{s,i} \text{ (hot period)} \quad (6)$$

$$T_g(L) = T_{e,i} \text{ (cold period)} \quad (7)$$

Furthermore, the heat transfer at the ends of the channel is assumed to be negligible [41], i.e.

$$\left.\frac{\partial T_m}{\partial x}\right|_{x=0} = \left.\frac{\partial T_m}{\partial x}\right|_{x=L} = 0 \quad (8)$$

The transient transport equations for the conservation of energy in the airflow and matrix are discretized using a finite volume method [42]. The upwind differencing and central differencing schemes are used to approximate the convection/diffusion terms in the airflow and the matrix, respectively. The resulting algebraic equation for the airflow is solved using a Gauss-Seidel iteration technique, where the Tridiagonal Matrix Algorithm (TDMA) is used to solve the energy equation in the matrix.

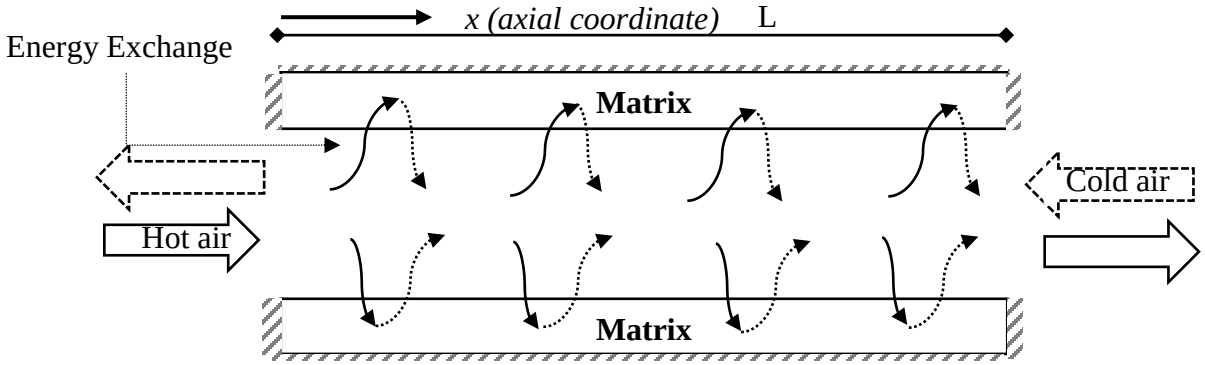

Fig. 6. Schematic of the numerical domain for heat transfer in the FBR channel (solid line for the hot period (hot air) and the dashed line for the cold period (cold air)).

4. Performance Parameters and Empirical Correlations

In this section, the performance parameters of FBRs and the empirical correlations used to validate the small-scale testing methodology will be presented and discussed in detail.

4.1. Performance parameters

Sensible effectiveness is one of the main parameters to assess the performance of regenerators. The sensible effectiveness of an FBR is defined as the ratio of the heat transfer rate between the exchanger and airstreams to the maximum possible heat transfer rate. The heat capacity rate of the working fluid, thermal properties of the exchanger materials, heat transfer area, and duration of heating and cooling periods are the factors that affect the sensible effectiveness. Eqns. (9) and (10) are used to determine the sensible effectiveness of a small-scale FBR for the

hot and cold periods, respectively [43]. Theoretically, the effectiveness determined using Eqns. (9) and (10) must be equal if there is no heat interaction between the exchanger and surroundings. However, in experiments, the measured data may vary due to experimental uncertainties even if there is no heat loss/gain from outside. Therefore the average of ε_{hot} and ε_{cold} is considered as the sensible effectiveness of small-scale FBR, which also reduces the experimental uncertainty [44].

$$\varepsilon_{hot} = \frac{C_1}{C_{min}} \times \frac{(T_1 - \overline{T}_2)}{(T_1 - T_3)} \tag{9}$$

$$\varepsilon_{cold} = \frac{C_2}{C_{min}} \times \frac{(\overline{T}_4 - T_3)}{(T_1 - T_3)} \tag{10}$$

where T_1 and T_3 are the temperatures of the hot and cold inlet air streams, and $\overline{T}_2$ and $\overline{T}_4$ are the time averaged air temperatures at the exchanger outlets respectively (Fig. 5). C_1 and C_2 are the heat capacity rates of hot and cold airstreams and C_{min} is the minimum of C_1 and C_2. Since the outlet temperature of the air streams varies with time, the time averaged outlet temperatures are determined using Eqn. (11) [43].

$$\overline{T} = \frac{1}{P}\int_0^P T(t)dt \tag{11}$$

where T is the instantaneous outlet air temperature and P is the total period.

The design and operating condition variables such as physical dimensions of the exchanger, face velocity and cycle period in small-scale experiments are different from that of practical FBRs. However, the sensible effectiveness can be represented as a function of two dimensionless parameters: number of transfer units (NTU_o) and heat capacity rate ratio (Cr^*) which includes the effects of these design and operating condition variables [43]. i.e. $\varepsilon = f(NTU_o \text{ and } Cr^*)$

$$NTU_o = \frac{UA}{C_{min}} \tag{12}$$

$$Cr^* = \frac{(\dot{m}C_p)_{matrix}/P}{(C_{min})_{air}} \tag{13}$$

where U is the overall heat transfer coefficient, A is the area of heat transfer, and C is the heat capacity rate respectively.

4.2 Empirical correlations

The operation of test facility and the testing methodology will be verified by comparing the test results with two empirical correlations proposed by Kays and London [43], and Buyukalaca and Yilmaz [45,46]. The Kays and London correlation is valid when the NTU_o and Cr^* is greater than or equal to one, whereas Buyukalaca and Yilmaz's correlation is valid for the entire range of NTU_o and Cr^*. However, latter was developed based on the experiments performed at low NTU_o and Cr^*; therefore it is expected to be more accurate at lower values of NTU_o's and Cr^*.

Kays and London's correlation has been developed by including two correction factors to the recuperative heat exchanger effectiveness by considering the effects of the period ($\emptyset$) and longitudinal heat conduction (φ) on heat transfer rate as shown in Eqn.(14).

$$\varepsilon_{reg} = \varepsilon_{CF} \cdot \emptyset \cdot \varphi \tag{14}$$

where, ε_{CF} is the effectiveness of a counter-flow heat exchanger and, for the same hot and cold air heat capacity rate, ε_{CF} can be determined using:

$$\varepsilon_{CF} = \frac{NTU_o}{1+NTU_o} \tag{15}$$

The correction factors $\emptyset$ and φ are determined using Eqns. (16) and (17).

$$\emptyset = 1 - \frac{1}{9\,(Cr^*)^{1.93}} \tag{16}$$

$$\varphi = 1 - \frac{C_\lambda}{2 - C^*} \tag{17}$$

where

$$C_\lambda = \frac{1}{NTU_o(1+\lambda\theta)/(1+\lambda \cdot NTU_o)} - \frac{1}{(1+NTU_o)} \tag{18}$$

where

$$\theta = \left(\frac{\lambda \cdot NTU_o}{1+\lambda \cdot NTU_o}\right)^{0.5} \tanh\left\{\frac{NTU_o}{[\lambda \cdot NTU_o/(1+\lambda \cdot NTU_o)]^{0.5}}\right\} \tag{19}$$

$$\lambda = \frac{K_m \cdot A_m}{L \cdot C_{min}} \tag{20}$$

where λ is known as longitudinal heat conduction factor and K_m, A_m and L are the thermal conductivity, cross-sectional area and length of the exchanger respectively.

Correlations for the longitudinal heat conduction factor agree within ±1% with the results of Bahnke and Howard's numerical solution [47] for $0 \leq \lambda \leq 0.08$.

The correlation for sensible effectiveness proposed by Buyukalaca-Yilmaz is given as [45,46]:

$$\varepsilon_{reg} = \frac{Cr^*}{\left\{1 + 3 \cdot \left(\frac{NTU_o \cdot Cr^*}{1 + NTU_o}\right)^2 + \left(\frac{NTU_o \cdot Cr^*}{1 + NTU_o}\right)^4\right\}^{0.25}} \quad (21)$$

In small-scale experiments, the flow within the exchanger is laminar. Therefore, the value of the convective heat transfer coefficient was taken from the literature based on the channel aspect ratio. The hydrodynamically and thermally developing length for the lowest face velocity (v= 0.8 m/s) are $^{X_{h,FD}}/_{L} = 0.2$ and $^{X_{th,FD}}/_{L} = 0.14$ which indicates that the flow becomes hydrodynamically and thermally developed fully only after 20% and 14 % of the total exchanger length respectively. Therefore the correlation of Nusselt number for simultaneously developing flow [48] was utilized to account the effects of both hydrodynamically and thermally developing flow on the heat transfer coefficient.

5. Results and Discussion

In this section, the test results at different operating conditions along with their uncertainty analysis are presented. The temporal and average outlet temperatures are analyzed and verified with the numerical model and correlations from the literature.

5.1. Temperature measurements and sensible effectiveness

During an experiment, the temperatures at the FBR outlets vary with time and reach a periodic profile when the experiment reaches quasi-steady state. The FBR outlet temperature profiles measured with the exchanger sensors and duct sensors are shown in Fig. 7 for hot and cold periods of 60 s and 15 s. During the hot period, the exchanger stores heat from the air (i.e. the cold matrix cools the hot air) and thus the air temperatures at the outlet are lower than at the inlet. The maximum heat transfer occurs at the beginning of the period and the outlet air temperature increases gradually as the cold exchanger is heated by the hot air. During the cold period, the exchanger releases the stored heat to the incoming cold air stream, resulting in heating of the cold inlet air.

Figure 7 shows that the temperature measured by the ducts and exchanger sensors are different at the beginning of each period but approach the same value at the end of each period. This deviation in the initial transient region (highlighted with dashed lines in Fig. 7 (a) and (b)) is due to the transient response of the thermocouples and the conditions at which the thermocouples were exposed during the previous period. Prior to the hot period shown in Fig.7 (a) (0-60 seconds),

the duct sensors were exposed to hot airstream and the exchanger sensors were exposed to cold airstream.

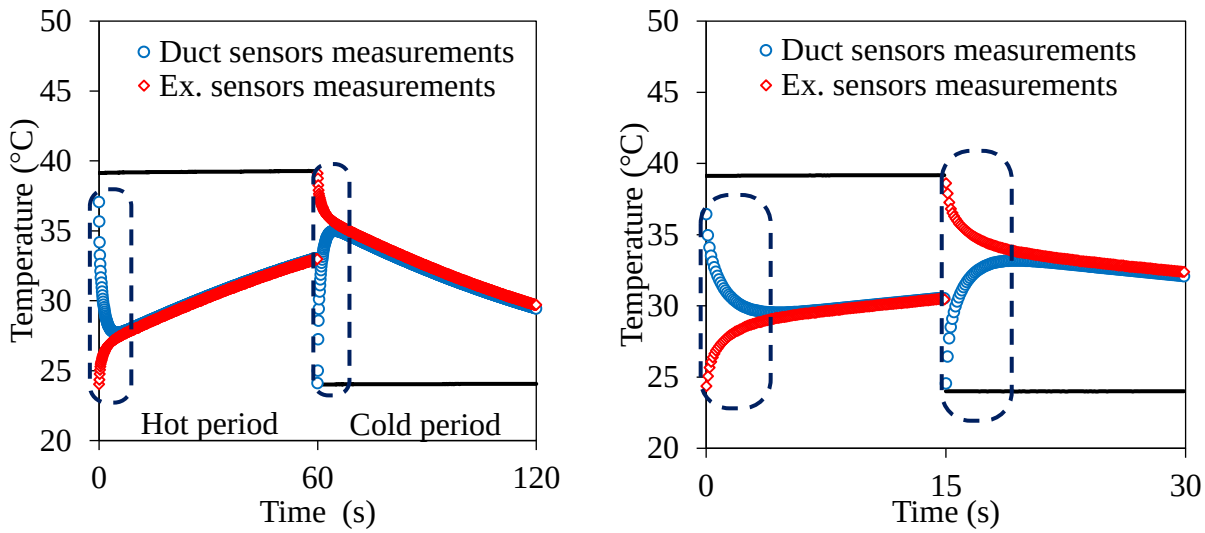

Fig. 7. Comparison of FBR outlet temperature profiles measured using duct sensors and exchanger sensors for hot and cold periods: (a) 60 s (Cr^*=1.12), and (b) 15 s (Cr^*=4.45) (Face velocity: 1.50 m/s, NTU_o= 2.25).

Therefore, these sensor measurements start from inlet hot and cold airstream temperatures respectively. When the period is 60 s, the duct and exchanger sensors take only 10% of the period to reach the same value within the experimental uncertainty. By comparison, when the period is 15 s the sensors take approximately 35% of the period to reach the same value.

The sensible effectiveness during hot and cold periods are determined from the average temperature over a period, Eqns. (10) and (11) can be defined over any period. The sensible effectiveness calculated from hot and cold period temperatures as a function of cycle number is shown in Fig. 8. At the beginning of experiment, the exchanger is at room temperature, the heat transfer rate between hot air and exchanger is greater, as compared to that of cold air and exchanger due to the large temperature difference between the exchanger and the hot airstream. Slowly, the exchanger attains a quasi-steady state where the heat transfer between both the airstreams and, exchanger becomes the same. The exchanger is assumed to operate in a quasi-steady state when the difference in hot side and cold side effectiveness is less than the uncertainty in sensible effectiveness for at least ten cycles.

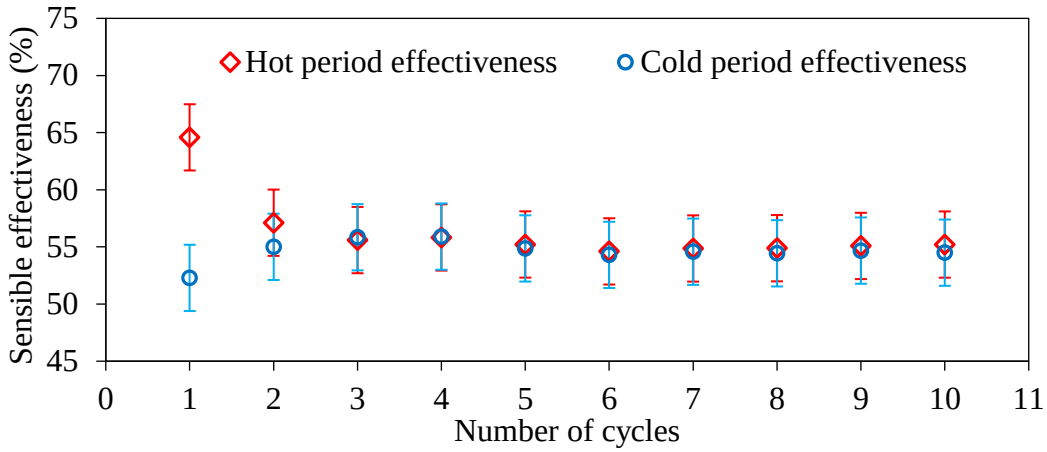

Fig. 8. Sensible effectiveness during hot and cold periods as a function of the number of cycles (NTU_o= 2.25 , Cr^*= 0.75).

The sensible effectiveness of FBR determined using exchanger and duct sensors after attaining a quasi-steady state is shown in Fig. 9. As explained previously, the transient response of the thermocouple causes incorrect temperature measurements at the beginning of each period, resulting in significant deviations in sensible effectiveness for periods less than 60 s.

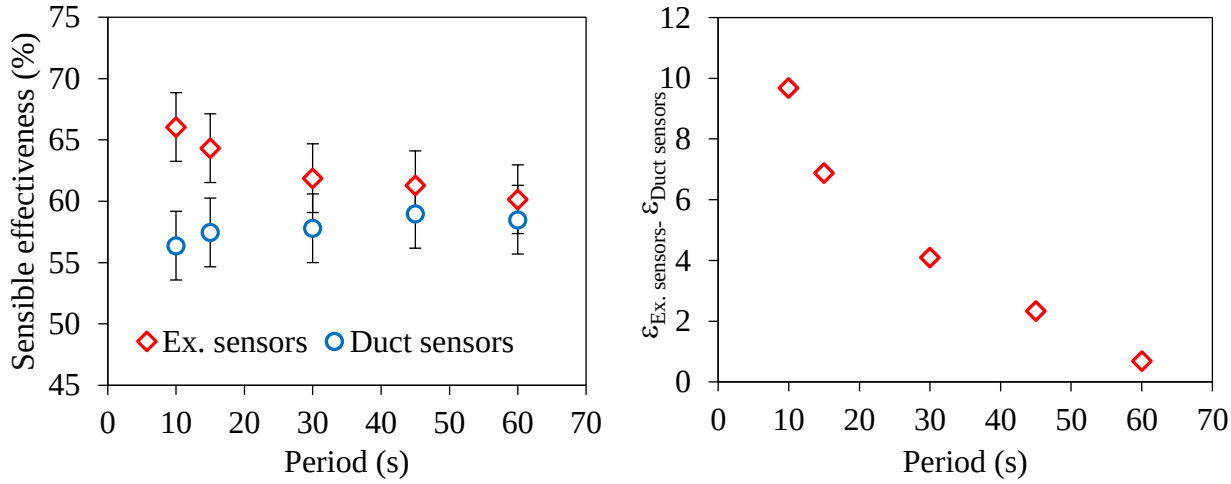

Fig. 9. (a) Comparison of sensible effectiveness determined from exchanger and duct sensors measurements and (b) their difference at different periods
(Face velocity: 1.5 m/s, NTU_o = 2.25)

For a period of 60 s, the sensible effectiveness determined from both the duct and exchanger sensors agree within the experimental uncertainty bound. By comparison, the sensible effectiveness determined from duct sensors and exchanger sensors have a 10% difference when

the exchanger operates with 10 s period. Therefore, the temperature measurements in FBR experiments become more critical for short operating periods.

Based on the experimental and numerical temperature profiles for several operating conditions (NTU_o 1.5 – 5 and Cr^* 1.5 – 7) it is found that the FBR outlet temperature varies linearly with time. Therefore, the initial temperature measurements are corrected by fitting a linear curve (linear backfit) on the final measurements in each period. The coefficient of determination R^2 is maintained to be at least 0.99. A sample temperature correction procedure is carried out on the exchanger sensors measurements and are shown in Fig. 10 (a) and comparison between the corrected experimental (Ex. corrected) and the numerical temperature profiles are shown in Fig. 10 (b).

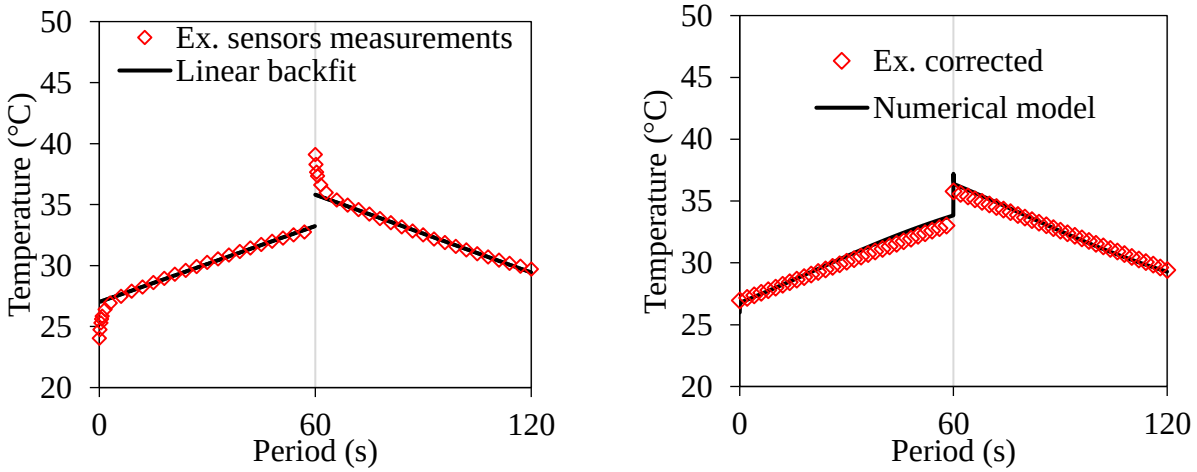

(a) (b)

Fig. 10. (a)Temperature profile correction on exchanger sensors measured data, and (b) the temperature profile at the FBR outlet obtained from experiment and numerical model (Face velocity: 1.5 m/s, NTU_o= 2.25, Cr^*= 1.12).

The average sensible effectiveness determined from corrected temperature measurements of both exchanger and duct sensors were compared with numerical results and are shown in Fig. 11. It can be observed that the results from both sensor arrangements are in good agreement with each other and with the numerical model.

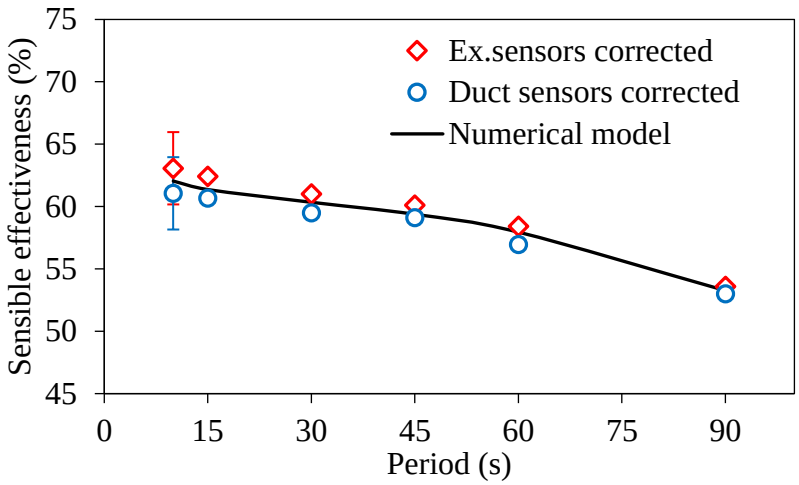

Fig. 11. Comparison of sensible effectiveness determined from corrected sensor measurements and the numerical model (Face velocity: 1.5 m/s, NTU_o: 2.25).

The maximum deviation of measurements between the exchanger and duct sensors from the numerical model is about 1.5% for a period of 10 s and this difference becomes less than 1.25% for 30, 60 and 90 s periods. Therefore, it is clear that, the back fit temperature correction can give accurate results even for a period of 10 s. Even though both sensor configurations can provide accurate results, the exchanger sensors are preferred over the duct sensors since they are located very close to the exchanger outlets. The results presented in the following sections are from the corrected temperature measurements of the exchanger sensors.

5.2. Test facility energy balance

It is necessary to perform energy balance in small-scale FBR facility in every experiment to ensure that the system is operating at a quasi-steady-state, (ie. the heat stored in the exchanger during the hot period is equal to the heat released by the exchanger during the cold period) and to ensure the heat exchange with surroundings is minimum.

During the quasi-steady state operation, in the absence of any heat losses and leakages from the test facility, the energy released from the exchanger during the cold period must be equal to the energy stored during the previous hot period. Sensible effectivenesses, determined from temperature measurements in both hot and cold periods (ε_{hot} and ε_{cold}), are used to analyze the energy balance since they represent a measure of energy transfer between the airstreams and the exchanger. The hot and cold period values of effectiveness, plotted in Fig. 12, show that ε_{hot} is generally 2 to 4% greater than that of ε_{cold}.

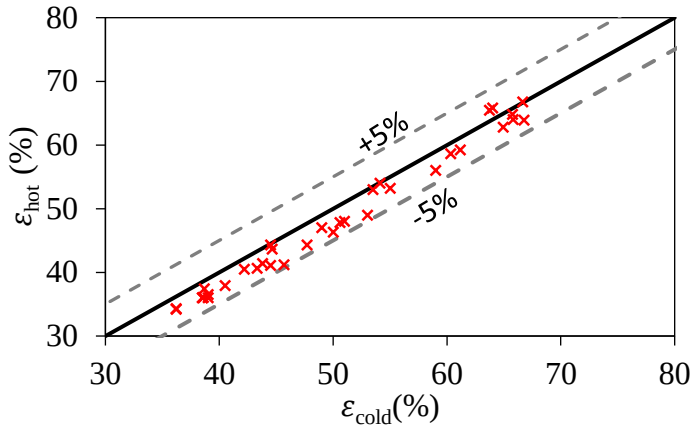

Fig. 12. Sensible effectiveness determined from hot and cold period temperature measurements for the tested operating conditions.

In all tested operating conditions, comparatively higher ε_{hot} than ε_{cold} values indicate the possibility of heat loss to the surroundings. This difference between the ε_{hot} and ε_{cold} is acceptable because the deviation is less than 5% for a wide range of tested conditions, uncertainty in sensible effectiveness varies from 2 to 4%, and the average of ε_{hot} and ε_{cold} is being considered as the performance measure of FBRs.

5.3. Effects of face velocity on sensible effectiveness

The sensible effectiveness of FBR varies with the inlet air stream velocity. The effect of face velocity on sensible effectiveness was studied by varying the face velocities from 1.0 to 1.7 m/s for a period of 60 seconds and results are shown in Fig. 13. The experiments were performed at balanced flow conditions, at which the flow rates of hot and cold airstreams are equal.

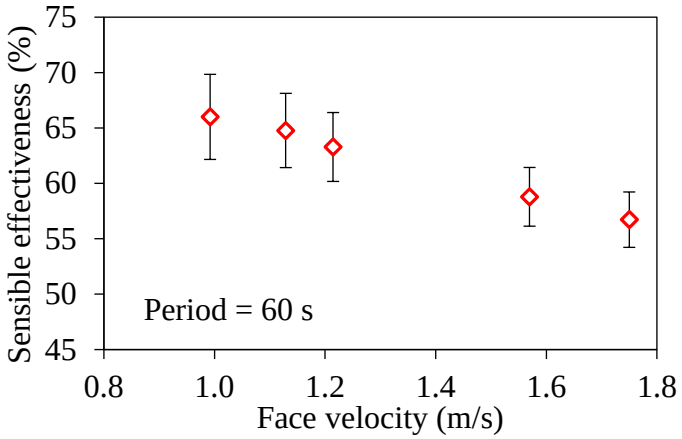

Fig. 13. Variation of sensible effectiveness with face velocity.

It can be seen that the sensible effectiveness decreases with an increase in face velocity. This is due to the fact that, at higher face velocities, the flow residence time of air inside the exchanger is less, which reduces the heat transfer. In other words, NTU_o is inversely proportional to the face velocity and hence lower NTU_o at higher face velocity lowers the sensible effectiveness.

5.4. Effects of period on sensible effectiveness

Period is one of the critical design parameters for FBR. In practical FBR units, the airflow direction is altered during each period with the help of dampers or valves. The life of dampers/valves is also an essential consideration since the frequent valve switching or damper movements can cause excessive wear and tear which leads to leakages and premature failures. Furthermore, excessive carry-over due to frequent switching also reduces indoor air quality. The usual operating period of FBRs ranges from 40 to 60 s based on optimum sensible effectiveness, acceptable indoor air quality and the valves or damper's switching ability [8].

The effect of period on sensible effectiveness was studied by performing experiments at a constant face velocity of 1.12 m/s at five different periods ranging from 10 to 60 s. From Fig. 14, it can be observed that sensible effectiveness increases with a decrease in period. This is mainly due to the fact that, the heat exchange between the air stream (hot/cold) and the exchanger is highest at the beginning of each period. As time proceeds, the heat transfer rate decreases and FBR reaches its maximum/minimum heat storage capacity which decreases the sensible effectiveness.

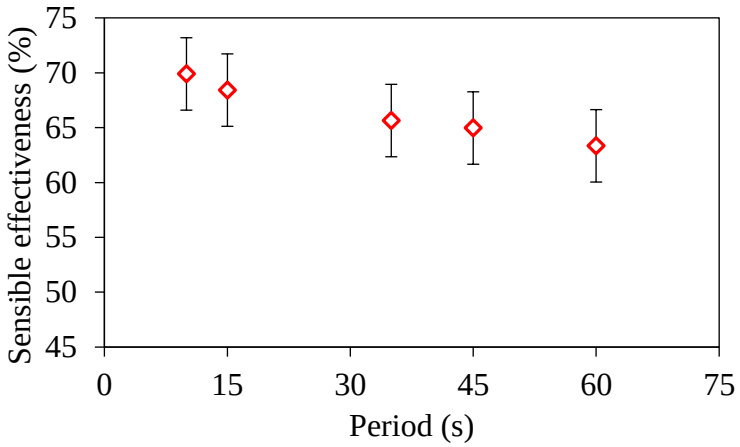

Fig. 14. Variation of sensible effectiveness with period (Face velocity: 1.12 m/s).

5.5. Comparison of test results with the numerical model and the empirical correlations

The test results from small-scale tests can not be applied directly to evaluate the performance of FBRs in practice since the operating conditions and physical dimensions of the

small-scale exchanger are different from that of real FBR units. Therefore, the tests were performed at different NTU_o and Cr^* conditions correspond to that of practical FBRs. These results are verified with the numerical model and empirical correlations proposed by Kays and London [43], and Buyukalaca and Yilmaz [45].

The results from the parallel-plate exchanger are used to verify the small-scale testing methodology at different NTU_o and Cr^* conditions. The tested range of operating conditions for constant NTU_o and Cr^* experiments are summarized in Table 3.

Table 3. The small-scale FBR test conditions.

Sl. No	T_h (°C)	T_c (°C)	NTU_o	$Re_{channel}$	Cr^*
1	39 ± 0.2	24.1 ± 0.2	1.5 - 5.0	262-850	2.1
2			2.25	500	0.75 – 6.8

The obtained sensible effectiveness for constant Cr^* and NTU_o operating conditions are shown in Fig. 15 and Fig. 16, respectively. The sensible effectiveness of FBRs increases with an increase in NTU_o and Cr^*. It can be seen that the results obtained from experiments are in good agreement with the numerical model and literature correlations at tested range of operating conditions. The maximum difference between experiment and numerical results is 2.3%. The uncertainty in measurements and the heat loss to surroundings could be the potential reasons for minor deviations in the experimental and numerical results.

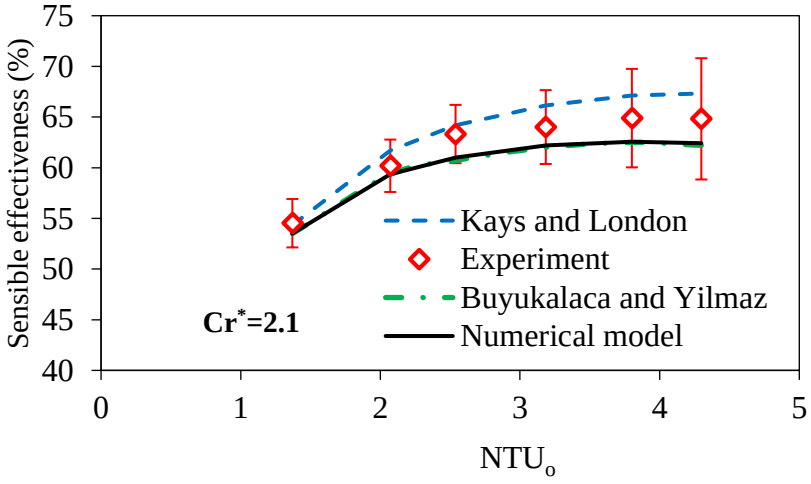

Fig. 15. Comparison of sensible effectiveness obtained from experiments with numerical model and two design correlations for a constant Cr^*.

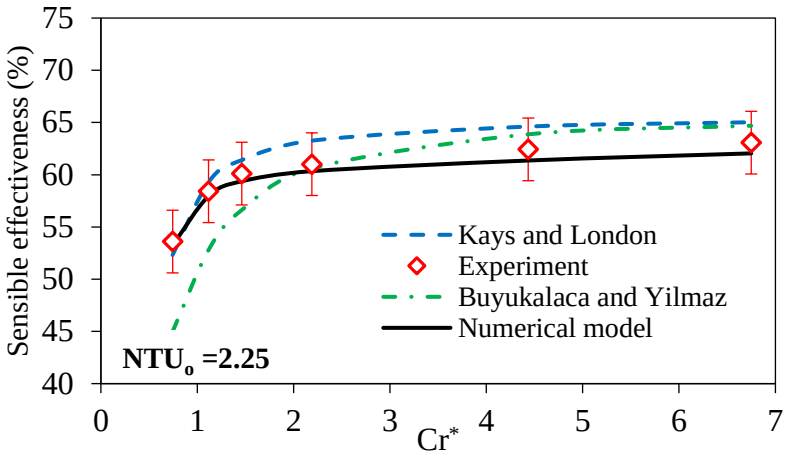

Fig. 16. Comparison of sensible effectiveness obtained from experiments with numerical model and two design correlations for a constant NTU_o.

The maximum difference between experimental results and Kays and London as well as and Buyukalaca and Yilmaz correlations are about 3% and 8%, respectively. It should be noted that the Buyukalca and Yilmaz have not included the effects of longitudinal heat conduction in their effectiveness correlation. Therefore the conduction parameter φ is determined from Eqns. (17) to (20) and applied in both Kays and London, and Buyukalaca and Yilmaz correlations. The deviations in the experimental results from the literature correlations were expected since the applicability of the longitudinal heat conduction parameter in the literature correlations affect the sensible effectiveness results. As described in Section 4.2, the correlation for the conduction parameter is validated for $0< \lambda<0.08$. However, for the tested operating conditions, λ varies from 0.2 to 0.68 (where the face velocities: 2.5 m/s and 0.8 m/s respectively).

As well, it should be noted that the literature correlations do not specify any uncertainty bounds for their results [21]. The Kays and London correlations are based on Lamberston's numerical model [38] which does not include any uncertainties. The correlation of Buyukalaca and Yilmaz were validated experimentally at low NTU_o and Cr^*operating conditions where they reported about 2.8-10% of deviation in sensible effectiveness for an increase in NTU_o from 1.26 to 2.31 [27,46]. Considering the close agreement between numerical results and the experiment results as well as the range of applicability of literature correlations, the small-scale testing methodology can be considered as a potential alternative option for performance evaluation of FBRs.

Full-scale FBRs with effectiveness more than 85% operate at NTU_o ranging from 5-8. In small-scale testing, to achieve higher NTU_o's, either the air face velocity needs to be decreased or the heat transfer area should be increased. At lower face velocities, the longitudinal heat conduction through the exchanger plates reduces the sensible effectiveness even at high NTU_o's (or reduces the effective NTU_o). Therefore, increasing the length of the exchanger is an effective way to test at higher NTU_o's compared to lowering the face velocity.

5.6. Uncertainty analysis

Another critical aspect to be addressed with alternative testing methods is the uncertainty in results. ANSI/ASHRAE 84-2013 [49] recommends a maximum uncertainty level of 5% for sensible effectiveness of energy exchangers. Therefore, the uncertainty levels of sensible effectiveness in any alternate testing methods should not exceed this limit. For the small-scale testing method presented herein, the uncertainty in sensible effectiveness comes from the systematic uncertainties in temperature and flow rate measurements. A detailed uncertainty analysis was carried out using the empirical correlation proposed by Kays and London [43] for a wide range of operating conditions. Sensible effectiveness of the small-scale exchanger presented in this study is estimated from the Kays and London correlation [43] at different operating conditions. Using this sensible effectiveness, the temperature of air at the FBR outlet is calculated from Eqn (4) and (5).The uncertainty in sensible effectiveness is finally determined by propagating the uncertainty in temperature and mass flow flowrate measurements using Eqn.(3). The temperature difference between hot and cold inlet airstreams is assumed to be 10°C for this analysis. The relative uncertainty in the mass flow rate at different face velocities was determined by propagating the bias error in pressure drop measurements using Eqn. (3) as shown in Fig. 17.

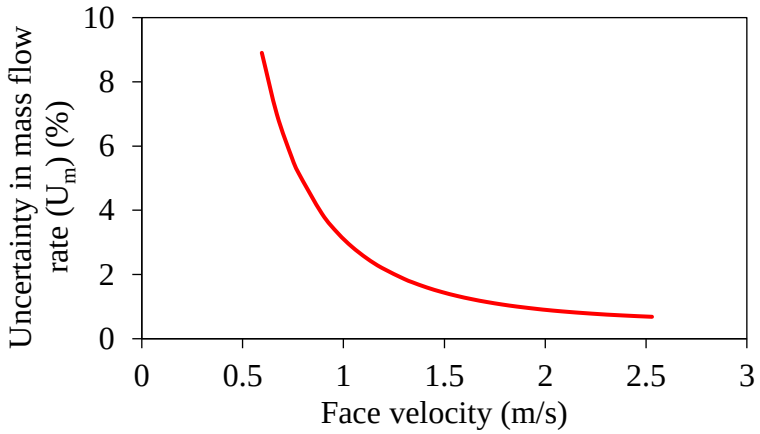

Fig. 17. Uncertainty in mass flow rate at different velocities.

As the face velocity decreases, the pressure drop across the orifice plate decreases and the relative uncertainty in the pressure drop measurement increases. The usual operating face velocities in FBRs are between 1-2.5 m/s, where the corresponding uncertainty in mass flow rates are determined as 3.1 to 0.6%. The contribution of uncertainties in mass flow rates and temperature measurements on the sensible effectiveness for NTU_o from 2-5 and the Cr^* from 0.5-5 are shown in Fig. 18 (a) and (b) respectively. The uncertainty in sensible effectiveness due to systematic error in mass flow rate increases with an increase in NTU_o. This because, for a given exchanger, the NTU_o can be increased only by reducing the mass flow rate. A decrease in mass flow rate results in an increase in uncertainty in pressure drop measurements (as shown in Fig. 17), which leads to higher uncertainty in the sensible effectiveness as NTU_o increases. The contribution of bias errors in temperature measurements is shown in Fig. 18 (b). It is clear that the uncertainty in sensible effectiveness due to bias error in temperature measurements increase slightly with an increase in NTU_o and Cr^*; however, these changes are less than 0.3%.

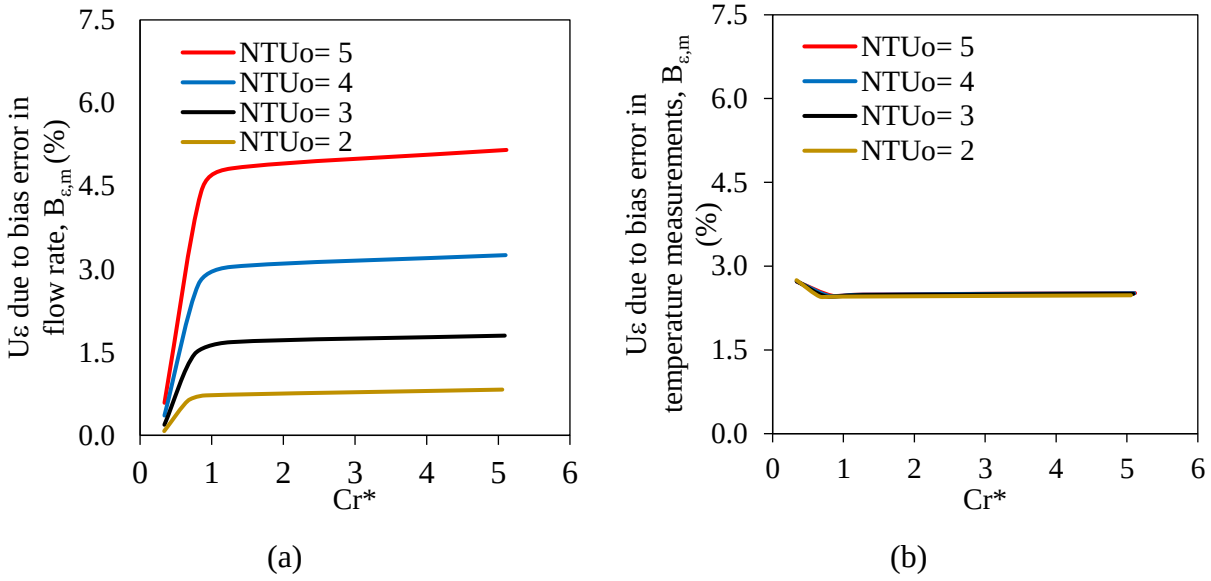

Fig. 18. Uncertainty in sensible effectiveness due to systematic uncertainty in (a) flow rate and (b) temperature measurements at different NTU_o and Cr^* conditions.

The overall uncertainty in sensible effectiveness by considering bias errors in both pressure drop and temperature measurements is shown in Fig. 19 (a). The increase in uncertainty in sensible effectiveness is significant with an increase in NTU_o compared to that of Cr*, which indicates that the uncertainty in flow rate measurements is more critical in overall uncertainty in sensible effectiveness. In addition, the uncertainty in sensible effectiveness is determined for the limiting

case of test facility (i.e., operating a 1m long exchanger at NTU_o's ranging from 2-5), where the result is shown in Fig. 19 (b).

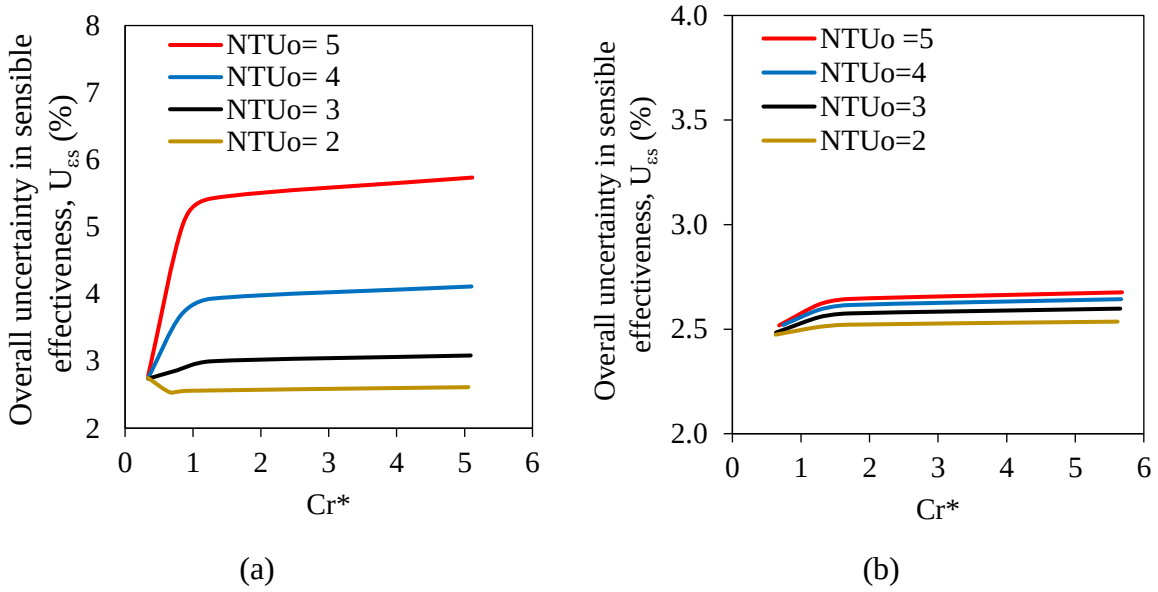

Fig. 19. Overall uncertainty in sensible effectiveness for 20 cm (a) and 1 m (b) long FBRs at different NTU_o and Cr^* conditions.

It is also noted that the Kays and London correlation [43] is validated for the conditions where Cr^* and NTU_o are higher than unity. Therefore, the uncertainty analysis results may not be accurate for the operating conditions having NTU_o and Cr* less than unity. Based on the uncertainty analysis, it can be concluded that the facility is capable of producing test results below the ANSI/ASHRAE 84-2013 [49] recommended uncertainty limits up to an NTU_o of 4.5 for a 20 cm long parallel-plate exchanger. It is also possible to test FBRs having length up to 1 m and generate results within ASHRAE recommended uncertainty limits Moreover, the uncertainties in small-scale testing can be further reduced by (i) decreasing the uncertainty in temperature and pressure drop measurements through equipment calibration, and (ii) reducing the uncertainty in flow rate measurements by changing the orifice plates according to the operating conditions.

6. Summary and Conclusions

This paper introduces a new small-scale test facility to investigate the performance of fixed-bed regenerators (FBRs) at different operating conditions. The facility is capable of testing exchangers having a length up to one meter, and the supply inlet air temperature and air velocity can be varied from -25 to 60°C and 0.8 to 2.5 m/s, respectively. The results from the small-scale

tests are presented using dimensionless performance parameters, where the FBR performance curves were plotted at constant NTU_o and Cr^* operating conditions. The errors in FBR outlet temperature measurements due to the transient response of sensors were corrected using a linear backfit method. A parametric study was performed to understand the influence of period and face velocity on sensible effectiveness of FBR.

The small-scale testing methodology is verified for FBRs by comparing the experimental results with the numerical model and two literature correlations for NTU_o and Cr^* from 1.5 to 5 and 1 to 6.5, respectively. The maximum difference in sensible effectiveness obtained from test results and the numerical model is 2.3%. When compared with the literature correlations, the experiment results are having a maximum deviation of 3% and 8 % with Kays and London, [43] and Buyukalaca and Yilmaz [46] correlations, respectively. These deviations are mainly because the value of the conduction parameter is outside the range of its applicability in the correlations. In addition, a detailed uncertainty analysis was performed and the contribution of each measurement to the overall uncertainty in sensible effectiveness was identified.The good agreement of test results with the numerical model, and low uncertainty in sensible effectiveness show that small-scale testing is a promising alternative methodology to evaluate the performance of FBRs. The test facility can be used to study the heat and moisture transfer in FBRs having different plate geometries and desiccant materials.

Acknowledgments

Financial support from the College of Engineering and Postdoctoral Studies of the University of Saskatchewan, National Science and Engineering Research Council (NSERC), Tempeff North America Inc., Winnipeg (Project No:533225-18) and the Government of Saskatchewan (Agriculture Development Fund, Project No: 20160266) are gratefully acknowledged. The support provided by Hayden Reitenbach and Shawn Reinink (Department of Mechanical Engineering, University of Saskatchewan) are also greatly appreciated.

References

[1] L. Pérez-Lombard, J. Ortiz, C. Pout, A review on buildings energy consumption information, Energy Build. 40 (2008) 394–398. doi:10.1016/j.enbuild.2007.03.007.

[2] A. Kasaeian, S.M. Hosseini, M. Sheikhpour, O. Mahian, W.M. Yan, S. Wongwises,

Applications of eco-friendly refrigerants and nanorefrigerants: A review, Renew. Sustain. Energy Rev. 96 (2018) 91–99. doi:10.1016/j.rser.2018.07.033.

[3] D. Enescu, A review of thermal comfort models and indicators for indoor environments, Renew. Sustain. Energy Rev. 79 (2017) 1353–1379. doi:10.1016/j.rser.2017.05.175.

[4] B.R.W. Besant, C.J. Simonson, Air-To-Air Energy Recovery, ASHRAE J. 42 (2000).

[5] F. Fathieh, M. Rafati Nasr, S. Sadeh, R.W. Besant, R.W. Evitts, J. Müller, C.J. Simonson, Determination of air-to-air energy wheels latent effectiveness using humidity step test data, Int. J. Heat Mass Transf. 103 (2016) 501–515. doi:10.1016/J.IJHEATMASSTRANSFER.2016.07.046.

[6] M. Justo Alonso, P. Liu, H.M. Mathisen, G. Ge, C. Simonson, Review of heat/energy recovery exchangers for use in ZEBs in cold climate countries, Build. Environ. 84 (2015) 228–237. doi:10.1016/j.buildenv.2014.11.014.

[7] R.W. Besant, C.J. Simonson, Air-to-air energy recovery, ASHRAE J. 42 (2000) 31–38.

[8] M. Rafati Nasr, F. Fathieh, D. Kadylak, R. Huizing, R.W. Besant, C.J. Simonson, Experimental methods for detecting frosting in cross-flow air-to-air energy exchangers, Exp. Therm. Fluid Sci. 77 (2016) 100–115. doi:https://doi.org/10.1016/j.expthermflusci.2016.04.009.

[9] M.A. El-Rifai, T. N.E., Temperature transients in fixed bed heat regenerators, Chem. Eng. Sci. 29 (1974) 1687–1694. doi:10.1016/0009-2509(74)87026-0.

[10] D.E. Marks, R.J. Robinson, C.W. Arnold, A.E. Hoffmann, Dynamic Behavior of Fixed-Bed Adsorbers, J. Pet. Technol. 15 (1963) 443–449. doi:10.2118/398-pa.

[11] Tempeff North America, The Dual Core Difference, (n.d.). https://www.tempeffnorthamerica.com/dual-core-heat-recovery/ (accessed August 21, 2019).

[12] V. Vakiloroaya, B. Samali, A. Fakhar, K. Pishghadam, A review of different strategies for HVAC energy saving, Energy Convers. Manag. (2014). doi:10.1016/j.enconman.2013.10.023.

[13] H. Ramin, E.N. Krishnan, C.J. Simonson, Fixed bed regenerators for HVAC applications, in: 27th Can. Congr. Appl. Mech., MDPI, Sherbrooke, 2019: pp. 1–6. doi:10.3390/proceedings2019023004.

[14] R. Kheiri, H. Ghaebi, M. Ebadollahi, H. Rostamzadeh, Thermodynamic modeling and

performance analysis of four new integrated organic Rankine cycles (A comparative study), Appl. Therm. Eng. 122 (2017) 103–117. doi:10.1016/j.applthermaleng.2017.04.150.

[15] H.R.B. Ajdari, S.M. Sadrameli, Theoretical and Experimental Studies of a Thermal Regenerator for Heat Recovery in Aluminum Melting Furnaces, in: M. Hyland (Ed.), Light Met. 2015, Springer International Publishing, Cham, 2016: pp. 439–443. doi:10.1007/978-3-319-48248-4_73.

[16] A. V. Koshel'nik, T.N. Pugachova, O. V. Kruglyakova, V.G. Pavlova, O. V. Dolobovskaya, Increasing the Operating Efficiency of Regenerative Heat-Exchangers of Glass Furnaces, Glas. Ceram. (English Transl. Steklo i Keramika). 76 (2019) 68–71. doi:10.1007/s10717-019-00134-1.

[17] C.C. Chang, J. De Liang, S.L. Chen, Performance investigation of regenerative total heat exchanger with periodic flow, Appl. Therm. Eng. 130 (2018) 1319–1327. doi:10.1016/j.applthermaleng.2017.11.024.

[18] C.H. Chen, P.C. Huang, T.H. Yang, Y.C. Chiang, S.L. Chen, Polymer/alumina composite desiccant combined with periodic total heat exchangers for air-conditioning systems, Int. J. Refrig. 67 (2016) 10–21. doi:10.1016/j.ijrefrig.2016.01.003.

[19] Y.A. Aristov, I. V Mezentsev, V.A. Mukhin, A new approach to heat and moisture regeneration in the ventilation system of rooms. I. Laboratory prototype of the regenerator, J. Eng. Phys. Thermophys. 79 (2006) 569–576. doi:10.1007/s10891-006-0137-7.

[20] M.I. Nizovtsev, V.Y. Borodulin, V.N. Letushko, A.A. Zakharov, Analysis of the efficiency of air-to-air heat exchanger with a periodic change in the flow direction, Appl. Therm. Eng. (2016). doi:10.1016/j.applthermaleng.2015.09.029.

[21] Canadian Standards Association, Standard Laboratory Methods of Test for Rating the Performance of Heat/Energy-Recovery Ventilators, CSA Group, Canada, 2018.

[22] M. Czachorski, J. Wurm, W.M. Worek, J. Mierke, P. Brillhart, Dynamic testing of desiccant matrices and computerized evaluation of performance maps, in: Am. Soc. Heating, Refrig. Air-Conditioning Eng. Winter Meet., American Society of Heating, Refrigerating and Air-Conditioning Engineers, Inc., Atlanta, GA (United States), United States, 1997: pp. 1–7. https://www.osti.gov/servlets/purl/345283.

[23] O.O. Abe, R.W. Besant, C.J. Simonson, W. Shang, Relationship between energy wheel speed and effectiveness and its transient response, part I: Mathematical development of the characteristic time constants and their relationship with effectiveness, in: ASHRAE Trans., 2006: pp. 103–115.

[24] F. Fathieh, A Novel Transient Testing Method for Heat/Energy Wheel Components, University of Saskatchewan, 2016. https://harvest.usask.ca/handle/10388/7381.

[25] O.O. Abe, Y.H. Wang, C.J. Simonson, R.W. Besant, W. Shang, Transient temperature measurements and characteristics for temperature sensors and energy wheels, in: ASHRAE Trans., 2006: pp. 76–89.

[26] Y. Wang, C.J. Simonson, R.W. Besant, W. Shang, Transient humidity measurements: Part I - Sensor calibration and characteristics, IEEE Trans. Instrum. Meas. (2007). doi:10.1109/TIM.2007.894881.

[27] F. Fathieh, R.W. Besant, R.W. Evitts, C.J. Simonson, Determination of air-to-air heat wheel sensible effectiveness using temperature step change data, Int. J. Heat Mass Transf. 87 (2015) 312–326. doi:10.1016/j.ijheatmasstransfer.2015.04.028.

[28] F. Fathieh, R.W. Besant, R.W. Evitts, C.J. Simonson, Effects of Heat Loss/Gain on the Transient Testing of Heat Wheels, (2016). doi:10.1115/1.4032762.

[29] M. Shakouri, E.N. Krishnan, L. Dehabadi, A.H. Karoyo, C.J. Simonson, L.D. Wilson, Vapor Adsorption Transient Test Facility for Dehumidification and Desorption Studies, Int. J. Technol. 9 (2018) 1092–1102. doi:https://doi.org/10.14716/ijtech.v9i6.230.

[30] M. Shakouri, E.N. Krishnan, A.H. Karoyo, L. Dehabadi, L.D. Wilson, C.J. Simonson, Water Vapor Adsorption–Desorption Behavior of Surfactant-Coated Starch Particles for Commercial Energy Wheels, ACS Omega. 4 (2019) 14378–14389. doi:10.1021/acsomega.9b00755.

[31] D.G. Moghaddam, P. Lepoudre, G. Ge, R.W. Besant, C.J. Simonson, Small-scale single-panel liquid-to-air membrane energy exchanger (LAMEE) test facility development, commissioning and evaluating the steady-state performance, Energy Build. 66 (2013) 424–436. doi:10.1016/j.enbuild.2013.07.017.

[32] D. Ghadiri Moghaddam, R.W. Besant, C.J. Simonson, A methodology for scaling a small-scale energy exchanger performance results to a full-scale energy exchanger, Int. J. Heat Mass Transf. 82 (2015) 555–567. doi:10.1016/j.ijheatmasstransfer.2014.11.040.

[33] ISO, International Standard: ISO 5167-1 Measurement of fluid flow by means of pressure differential devices inserted in circular cross-section conduits running full--Part 1: General principles and requirements, Geneva, 2003.

[34] ISO, International Standard: ISO 5167-2, Measurement of fluid flow by means of pressure differential devices inserted in circular cross section conduits running full--part 2 Orifice plates, Geneva, 2003.

[35] Hart Scientific, 9105 / 9107 Dry-well Calibrator User's Guide, Utah, 2002.

[36] Thunder Scientific® Corporation, Model 1200 Mini "Two-Pressure" Humidity Generator., (n.d.). https://www.thunderscientific.com/humidity_equipment/model_1200.html (accessed June 21, 2018).

[37] G. Druck, DPI 605 Precision Portable Pressure Calibrator, (n.d.). http://www.testequipmentdepot.com/druck/pressure-calibrators/dpi605.htm (accessed August 19, 2019).

[38] ASME/ANSI, Performance Test Code 19.1 Test Uncertainty: Instruments and Apparatus, New York, 1998.

[39] R.S. Figliola; D.E. Beasley, Theory and Design for Mechanical Measurements, 4th ed., John Wiley & Sons Inc, Hoboken, New Jersey, 2006.

[40] C.J. Simonson, R.W. Besant, Heat and moisture transfer in desiccant coated rotary energy exchangers: Part I - numerical model, ASHRAE Trans. 104 (1998) 229.

[41] C.J. Simonson, R.W. Besant, Energy wheel effectiveness: Part I-development of dimensionless groups, Int. J. Heat Mass Transf. 42 (1999) 2161–2170. doi:10.1016/S0017-9310(98)00325-1.

[42] H.K. Versteeg, W. Malalasekera, An introduction to computational fluid dynamics : the finite volume method, 6th ed, Pearson Education Ltd., England, 2007.

[43] R.K. Shah, D.P. Sekulic, Fundamentals of Heat Exchanger Design, John Wiley & Sons, Inc., Hoboken, NJ, USA, 2003. doi:10.1002/9780470172605.

[44] C.J. Simonson, C. Dustin, R.W. Besant, Determining the performance of energy wheels: Part 1 - Experimental and numerical methods, ASHRAE Trans. 105 (1999) 174–187.

[45] O. Büyükalaca, T. Yilmaz, Influence of rotational speed on effectiveness of rotary-type heat exchanger, Heat Mass Transf. 38 (2002) 441–447. doi:10.1007/s002310100277.

[46] T. Yilmaz, O. Büyükalaca, Design of regenerative heat exchangers, Heat Transf. Eng. 24 (2003) 32–38. doi:10.1080/01457630304034.

[47] G.D. Bahnke, C.P. Howard, The effect of longitudinal heat conduction on periodic-flow heat exchanger performance, J. Eng. Gas Turbines Power. 86 (1964) 105–117. doi:10.1115/1.3677551.

[48] Shah R.K, London A.L, Advances in Heat Transfer, Laminar Flow Forced Convection in Ducts, Academic Press, New York, 1978.

[49] ASHRAE, ASHRAE standard 84-2013, Method of Testing Air-to-Air Heat/Energy Exchangers, ASHRAE, Atlanta, 2013.